(Preprint) AAS 23-166

ADVANCED GUIDANCE DESIGN VIA SUCCESSIVE CONVEX OPTIMIZATION FOR THE 6-DOF ATMOSPHERIC RE-ENTRY OF REUSABLE LAUNCHERS

Alice De Oliveira[*] and Michèle Lavagna[†]

This paper studies the development, analysis and improvement of a successive convex optimization guidance algorithm which solves the 6-DoF powered-descent fuel-optimal control problem for reusable launchers re-entry. An analysis is carried out to find the optimal trajectory problem formulation that leads to the best performance results. More particularly, the minimum-time strategy is compared with the maximization of the final mass as well as the minimization of the thrust usage throughout the flight. Performance is also evaluated comparing the convexification methods such as lossless convexification or 1st-order Taylor expansion approximation. Advanced state and control constraints are studied such as aerodynamics and thrust slew rate. Finally, the guidance system is embedded in a nonlinear simulator to assess the global performance.

INTRODUCTION

The controlled atmospheric re-entry associated with the precision soft-landing of Reusable Launch Vehicles (RLVs) on Earth is very challenging as it depends on multiple parameters.[1] Over the last decade, the cost-effectiveness of such a technology has been finally demonstrated with the successful recoveries of SpaceX's Falcon 9 first-stage rocket first,[2] then followed by other companies such as the Rocket Lab's Electron microlauncher.[3] Today, SpaceX has flown reusable boosters more that 100 times, with some single boosters reused more than 10 times, proving the feasibility and the economic sustainability of such a technology. This breakthrough has been made possible by the development of advanced and robust computational methods able to generate in real time the reference trajectory to be followed according to the flight conditions, and to output the optimal vehicle's deflections accordingly to steer the vehicle toward this trajectory until a safe pinpoint landing.

Indeed, during an Earth atmospheric re-entry, the vehicle is subjected to fast system dynamics changes partly induced by external loads associated with the terrestrial environment (e.g., lift, drag, wind and gusts), but also by the actuation commands to answer the landing constraints satisfaction and the vehicle integrity preservation. All those involve uncertainties and nonlinearities, which lead to vehicle's instability and therefore justify the implementation of a highly performant Guidance, Navigation and Control (GNC) system.[4] More particularly, one of the critical aspects is the design of an advanced guidance algorithm capable of generating in real time and rapidly valid solutions but also to possibly consider significant off-nominal conditions experienced during the descent flight.

[*]Ph.D. student, Department of Aerospace Science and Technology, Politecnico di Milano, via Giuseppe la Masa 34, 20156, Milan, Italy.

[†]Full professor, Department of Aerospace Science and Technology, Politecnico di Milano, via Giuseppe la Masa 34, 20156, Milan, Italy.

On the other hand, the pinpoint landing requirement involves a high accuracy and a perfect coordination between thrust, position, velocity, and attitude to enable a vertical and soft touchdown at the desired landing site.[5]

Research in the area of optimal aerodynamic and powered-descent trajectory generation began with the Apollo program in which a polynomial guidance scheme for the acceleration profile was computed offline according to the initial and final desired positions and velocities.[6] Nevertheless, this method did not consider fuel-optimality, neither allowed for further constraints inclusion. Then, the Space Shuttle entry guidance method used a reference drag-velocity profile to control bank angle and angle of attack during the descent,[7] which allowed to better consider the constraints involved (dynamic pressure, heat flux, load factor). However, thanks to the increase of computational power available on board, the recent progresses have shown that convex optimization is the key technology to enable autonomous and onboard real-time trajectory planning and therefore pinpoint landing. It consists of transforming the nonlinear re-entry trajectory problem into a convex one, more precisely into a Second Order Cone Programming (SOCP) problem, which can be solved with efficient solvers in polynomial time. More particularly, the lossless convexification of the nonconvex thrust magnitude lower bound constraint first,[8] and then further constraints, had made possible the successful pinpoint landing of the Masten Space Systems' Xombie sounding rocket in 2012[9] and the SpaceX's Falcon 9 in 2015.

Among the convex optimization family of methods, successive convex optimization has emerged as an effective approach to transition from a fully convex 3-DoF to a 6-DoF problem with some nonconvexity[10] but also to account for nonlinearities and additional constraints, more particularly the aerodynamic forces which can be included in the control authority.[11] Moreover, this problem formulation allows to reduce (both in terms of time and cost) the Verification and Validation campaign for which it used to be necessary to check that the 3-DoF trajectory is executable in a fundamentally 6-DoF lander system. Since the mid 2010s, several studies have been achieved in successive convex optimization. In certain cases, lossless convexification is embedded to remove some nonlinearity, and aerodynamic drag and even lift are approximated. Other developments enable the advent of State-Triggered Constraints (STC), embedding an if-then logic into the guidance problem, and allowing the definition of new constraints such as for example a velocity-triggered angle of attack constraint or a range-triggered line-of sight constraint.[12] Finally, simultaneously, research on embedding pseudospectral discretization in the problem formulation have emerged with more particularly the development of the successive pseudospectral convex optimization method, yielding to greater accuracy and faster solutions.[13]

This paper studies the development, analysis, and improvement of a successive convex optimization guidance algorithm, adapted from (Reference 12). This algorithm solves the 6-DoF powered-descent guidance problem with free final time, nonlinear dynamics with aerodynamic drag and nonconvex constraints. More particularly, it is using a spherical aerodynamic model which allows drag generation, approximating the nonlinearities and nonconvexities through first-order Taylor expansions and considering a dynamic pressure-triggered angle of attack constraint. Moreover, to better assess the algorithm performance, the guidance logic is embedded in a closed-loop fashion in a nonlinear 6-DoF RLV re-entry dynamics simulator with a control system using gain-scheduled Proportional-Integral-Derivative (PID) controllers. It covers the atmospheric re-entry and vertical landing of a first-stage rocket equipped with a Thrust Vector Control (TVC) system and steerable planar fins.[14]

Several algorithm developments are investigated, more particularly regarding the selection of

the cost function, the convexification method and the set of penalization weights for trust regions and virtual controls. In fact, the minimum-time strategy is compared with the maximization of the final mass as well as the minimization of the thrust usage throughout the flight. The lossless convexification method is compared with the 1st-order Taylor expansion approximation. Finally, the ability of the algorithm to counteract realistic aerodynamics is assessed. All these cases are carried out using the nonlinear simulator and the obtained performance are analyzed towards the selection of the best design. For this purpose, first the RLV re-entry controlled dynamics simulator is introduced with all the flight mechanics involved. Then, the guidance problem is defined and the successive convex optimization method is explained. Following, the different algorithm developments are described and assessed inside the guidance logic. After the selection of the best-performing cases, they are embedded in a closed-loop fashion with the nonlinear RLV reentry simulator to be tested in a realistic scenario. Finally, a summary of the paper and its main conclusions are presented.

REUSABLE LAUNCHERS RE-ENTRY CONTROLLED DYNAMICS SIMULATOR

This section describes the nonlinear 6-DoF dynamics of a Vertical Take-off Vertical Landing (VTVL) vehicle first-stage booster modelled as a rigid body with varying mass, subjected to external forces induced by the terrestrial atmosphere and controlled through embedded closed-loop guidance and control strategies.

This paper relies on the 6-DoF reusable launchers re-entry controlled dynamics simulator developed by the authors to study the efficiency of aerodynamic steering and conventional Guidance and Control (G&C) techniques.[14] Whereas in this previous research work, the vehicle was only steered via a TVC system and the fixed planar fins implementation was studied, the RLV simulator used in this paper considers a vehicle actuated both by the TVC system and steerable planar fins. An analysis to add an enhanced aerodynamic model in the simulator was also carried out.[15] Figure 1 describes the architecture of the simulator with the interactions between all the building blocks; from G&C systems to actuators, vehicle dynamics, and environment.

The simulator includes standard G&C algorithms where a thrust vector is commanded by the guidance subsystem and then converted to reference pitch $\theta_{ref}(t)$ and yaw $\psi_{ref}(t)$ angles, and thrust magnitude T_{ref}. Then, the control subsystem generates the necessary commands to correct

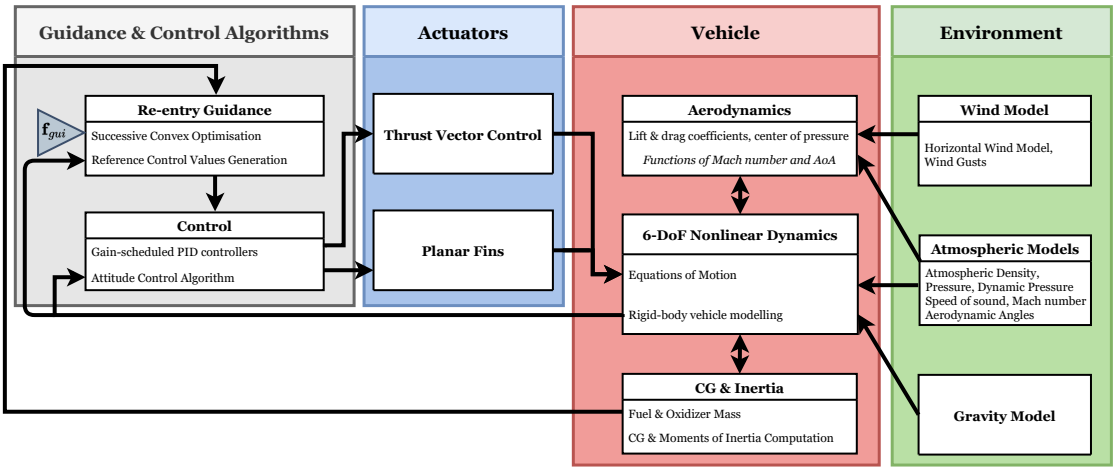

Figure 1: 6-DoF RLV Re-entry Controlled Dynamics Simulator Description

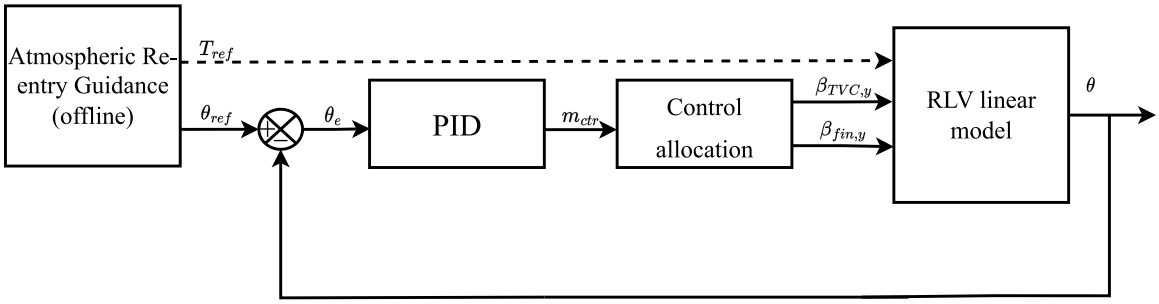

Figure 2: Structure for Baseline Control Synthesis, adapted from (Reference 4).

the deviations between the reference and actual attitude angles in terms of TVC gimbal deflections $\{\beta_{TVC,y}, \beta_{TVC,z}\}$ and fins' deflections $\{\beta_{fin,y}, \beta_{fin,z}\}$. The guidance subsystem relies on a successive convex optimization algorithm which consists in iteratively solving convex optimization SOCP subproblems in which the nonconvex dynamics and constraints are repeatedly linearized using the information coming from the previous iteration solution. The generated reference trajectory is updated with a user-specified frequency f_{gui} at which the guidance subsystem is re-executed. Concerning the control subsystem, it relies on the use of feedback control though gain-scheduled PID controllers, decoupling pitch and yaw axes based on the assumption of low roll rates. To simplify the MIMO formulation due to the consideration of TVC and steerable planar fins, for which it is complex to apply classical linear control theory, a control moment is defined as a variable specifying the necessary pitch or yaw moment to be commanded to correct the trajectory of the vehicle, following the work in (Reference 4). Then, knowing the control effectiveness level of each actuator, a control allocation algorithm is used to determine the actual control inputs in terms of TVC gimbal and fins' deflection angles. Figure 2 illustrates this structure for the gain-scheduled PID controllers synthesis, where a reference trajectory corresponding to the simulated case is stored offline and used through the RLV linear model to tune the scheduled PID controllers by sampling the system in n different points according to the altitude.

The equations of motion are written in the landing site-centered inertial and the vehicle's body-fixed reference frames based on the initial state $\mathbf{x}_I(0) = \begin{bmatrix} m(0) & \mathbf{r}_I^T(0) & \mathbf{v}_I^T(0) & \mathbf{q}_B^I(0)^T & \boldsymbol{\omega}_B^T(0) \end{bmatrix}$ and on the assumptions that the vehicle is a rigid body with no effect induced by the varying mass (e.g. propellant sloshing) and structural flexibilities for the sake of simplicity. Therefore we can formulate the 6-DoF re-entry equations of motion of a powered RLV as described by the following set of nonlinear differential equations summarized in Eq. (1).

$$
\begin{aligned}
\dot{m}(t) &= -\frac{||\mathbf{F}_{TVC,I}(t)||_2}{I_{sp} g_0} - \frac{A_{nozzle} P_{amb}(t)}{I_{sp} g_0} \\
\dot{\mathbf{r}}_I(t) &= \mathbf{v}_I(t) \\
\dot{\mathbf{v}}_I(t) &= \frac{1}{m(t)} \left[\mathbf{F}_{TVC,I}(t) + \mathbf{F}_{fins,I}(t) + \mathbf{F}_{aero,I}(t) \right] + \mathbf{g}_I(t) \\
\dot{\mathbf{q}}_B^I(t) &= \frac{1}{2} \begin{bmatrix} q_4(t) & -q_3(t) & q_2(t) \\ q_3(t) & q_4(t) & -q_1(t) \\ -q_2(t) & q_1(t) & q_4(t) \\ -q_1(t) & -q_2(t) & -q_3(t) \end{bmatrix} \boldsymbol{\omega}_B(t) \\
\dot{\boldsymbol{\omega}}_B(t) &= J^{-1}(t) \left[\mathbf{M}_{TVC,B}(t) + \mathbf{M}_{fins,B}(t) + \mathbf{M}_{aero,B}(t) - \boldsymbol{\omega}_B(t) \times J \boldsymbol{\omega}_B \right]
\end{aligned}
\tag{1}
$$

In Eq. (1), $m(t)$ is the mass of the vehicle, $\mathbf{r}_I(t) \in \mathbb{R}^3$ and $\mathbf{v}_I(t) \in \mathbb{R}^3$ are the position and velocity at the center-of-gravity (CG) of the vehicle expressed in the inertial reference frame. The attitude states are governed by the quaternion-based kinematics equation where $\boldsymbol{\omega}_B(t) \in \mathbb{R}^3$ is the angular velocity vector expressed in the vehicle's body-fixed reference frame. I_{sp} is the vacuum specific impulse of the engine, g_0 is the standard Earth gravity, A_{nozzle} is the nozzle exit area of the engine, $P_{amb}(t)$ is the ambient atmospheric pressure and $J(t) = \text{diag}\left(\begin{bmatrix} J_A(t) & J_N(t) & J_N(t) \end{bmatrix}\right)$ is the inertia matrix of the vehicle. The terms $\mathbf{F}_{aero,I}(t) \in \mathbb{R}^3$ represent the aerodynamic force of the vehicle expressed in the inertial reference frame; $\mathbf{F}_{TVC,I}(t) \in \mathbb{R}^3$, and $\mathbf{F}_{fins,I}(t) \in \mathbb{R}^3$ represent the control forces generated by the TVC system and the steerable planar fins, respectively. Equivalent to the forces, $\mathbf{M}_{aero,B}(t) \in \mathbb{R}^3$, $\mathbf{M}_{TVC,B}(t) \in \mathbb{R}^3$, and $\mathbf{M}_{fins,B}(t) \in \mathbb{R}^3$ represent aerodynamic and control moments written in the vehicle's body-fixed reference frame.

For the computation of the aerodynamic forces and moments, it is necessary to define an additional reference frame, the so-called velocity reference frame. This latter is fixed to the vehicle's CG with its x-axis directed along the wind-relative vector $\mathbf{v}_{air}(t)$ so that the transformation from the body-fixed to the velocity reference frame can be represented by two aerodynamic angles: the angle of attack $\alpha(t)$, and the sideslip angle $\beta(t)$.[16] Then the aerodynamic characteristics depend on the vehicle's external shape with its reference area and on the instantaneous dynamic pressure, which is defined as follows:

$$Q(t) = \frac{1}{2}\rho(t)||\mathbf{v}_{air}(t)||^2 \tag{2}$$

where $\mathbf{v}_{air}(t)$ accounts for the vehicle's inertial velocity and wind gusts; and the atmospheric density $\rho(t)$ is generated using the Committee on Extension to the Standard Atmosphere model[17] (like the ambient pressure $P_{amb}(t)$).The aerodynamic drag and lift coefficients, as well as the center of pressure, are estimated from lookup tables as function of the effective angle of attack $\alpha_{eff}(t) = \sqrt{\alpha^2(t) + \beta^2(t)}$ and the Mach number $M(t)$.[15]

Then, the gravitational field is defined in the inertial frame as a function of the altitude $r_{I,x}(t)$:

$$\begin{aligned} \mathbf{g}_I(r_{I,x}(t)) &= \begin{bmatrix} g(r_{I,x}(t)) & 0 & 0 \end{bmatrix}^T \\ g(r_{I,x}(t)) &= g_0 \left(\frac{R_E}{R_E + r_{I,x}(t)} \right)^2 \end{aligned} \tag{3}$$

where R_E is the radius of the Earth.

GUIDANCE PROBLEM VIA SUCCESSIVE CONVEX OPTIMIZATION

For the RLV re-entry simulator introduced in the previous section, the guidance algorithm is responsible for the real-time generation of a reference trajectory to be followed by the vehicle with thrust and attitude commands. Here, a direct method is used among the framework of convex optimization. This latter consists in transforming the fuel-optimal trajectory problem into a convex one, more precisely into a SOCP problem, which can be solved with efficient solvers in polynomial time. The challenging tasks rely in converting nonconvex state and control constraints into the convex form and on the high computational power needed. Recently, the so-called lossless convexification method[8] and the progresses in computational development have enabled to overcome these issues, and therefore to enable real-time trajectory generation in a closed-loop fashion.

Moreover, a particular class of convex optimization, successive convex optimization, can be applied to approximate the remaining nonlinearities in the optimal landing problem such as the aerodynamic effects, previously ignored. It consists in iteratively solving convex optimization SOCP

subproblems in which the nonconvex dynamics and constraints are repeatedly linearized using information coming from the previous iteration solution. This algorithm has been first developed in (Reference 18) and then adapted in different ways.[11,19] In this paper, the successive convex optimization algorithm adapted relies on the work achieved in (Reference 20) where the strategy defined in (Reference 12) was enhanced to be applicable in a closed-loop fashion towards a 6-DoF re-entry dynamics simulator.

For this study, the successive convex optimization guidance algorithm has been implemented in MATLAB using the CVX library[21] to formulate the convex problem and the ECOS routine[22] to solve them. At each simulation instance defined by the simulation rate $f_{sim} = 0.001$ Hz, the reference thrust profile $\mathbf{T}_{B,ref}(t)$ and the reference attitude angles $\{\theta_{ref}(t), \psi_{ref}(t)\}$ are computed from the most recent guidance solution via linear interpolation. Indeed, that solution is stored as an online lookup table which is updated at each guidance step, with the guidance update frequency $f_{gui} = 0.1$ Hz, so every 10 seconds. To enable the formulation of the SOCP subproblems, the optimal control problem must be converted into a finite dimensional parameter optimization problem. Therefore, the trajectory and optimization variables are discretized into K uniformly spaced points. At each guidance step, the time vector is divided in that way:

$$t_k = \frac{k-1}{K-1} t_f, \quad k \in [1, K] \tag{4}$$

and because the estimated time of flight $t_f \to 0$ as $t \to ToF$, where ToF is the actual time of flight achieved by the simulation, the accuracy of the discretisation becomes more precised towards the end.

Therefore, to compute the optimal reference trajectory to be followed, several state and control constraints are considered in addition to the re-entry dynamics. Regarding the state constraints, the first one is a lower bound of the mass: for each time instant $t_k,\ k \in [1, K]$, the mass cannot be lower than the dry mass of the vehicle ($m_{dry} = 2,750$ kg). This constraint is expressed by:

$$m[k] \geq m_{dry} \tag{5}$$

The second constraint is the so-called glide-slop constraint: it restricts the inertial position to lie within a glide-slope cone with half-angle $\gamma_{gs} \in [0, 90 \text{ deg})$ and vertex at the landing site. This constraint is enforced by:

$$\mathbf{e}_1 \cdot \mathbf{r}_I[k] \geq \tan(\gamma_{gs}) \left|\left| \begin{bmatrix} \mathbf{e}_2 & \mathbf{e}_3 \end{bmatrix}^T \mathbf{r}_I[k] \right|\right|_2 \tag{6}$$

where $\mathbf{e}_i,\ i \in [1, 3]$ are the versors. For this study, $\gamma_{gs} = 10 \text{ deg}$. Then, the third constraint concerns the tilt angle, i.e. the angle between the $\mathbf{x}$-axes of the two reference frames, which is bounded to be less than a maximum $\theta_{max} \in (0, 90 \text{ deg}]$. Here, $\theta_{max} = 75 \text{ deg}$. It is defined by:

$$\cos(\theta_{max}) \leq \mathbf{e}_{I,1}^T \mathbf{R}_I^B[k] \mathbf{e}_{B,1} \tag{7}$$

Then, the fourth constraint limits the angular rate of the vehicle to $\omega_{max} = 28.6 \text{ deg}$, it is enforced by:

$$||\boldsymbol{\omega}_B[k]||_2 \leq \omega_{max} \tag{8}$$

Finally, an additional constraint preserves the unit norm of the quaternion, as follows:

$$||\mathbf{q}_B^I[k]|| = 1 \tag{9}$$

Boundary constraints are added regarding initial and desired final conditions. Note that the initial attitude has not been constrained for the first guidance iteration while it was when the problem is solved during the flight to preserve the continuity of the solution. Moreover, a so-called STC[12] is added. In that case, it consists in imposing an angle of attack α constraint, α_{max}, when the dynamic pressure $Q(t)$ is larger than a prescribed value Q_{max}. The values $\alpha_{max} = 5$ deg and $Q_{max} = 4 \cdot 10^4$ Pa were chosen. This constraint is written in a continuous formulation with a *trigger*-function g_α and a *constraint*-function c_α as follows:

$$\begin{aligned} h_\alpha(\mathbf{r}_I[k], \mathbf{v}_I[k], \mathbf{q}_B^I[k]) &= -\min(g_\alpha(\mathbf{v}_I[k], \mathbf{r}_I[k]), 0) \cdot c_\alpha \leq 0 \\ c_\alpha(\mathbf{v}_I[k], \mathbf{q}_B^I[k]) &= \mathbf{e}_1 \cdot \mathbf{R}_B^I[k]\mathbf{v}_I[k] + \cos(\alpha_{max})||\mathbf{v}_I[k]||_2 \\ g_\alpha(\mathbf{r}_I[k], \mathbf{v}_I[k]) &= Q_{max} - \frac{1}{2}\rho[k]||\mathbf{v}_I[k]||_2^2 \end{aligned} \tag{10}$$

Finally, two control constraints are considered to bound the direction and magnitude of the thrust force. The direction is bounded by limiting the TVC up to a maximum gimbal angle $\delta_{max} = 10$ deg. It is enforced by:

$$\cos(\delta_{max})||\mathbf{T}_{B,ref}[k]||_2 \leq \mathbf{e}_1 \cdot \mathbf{T}_{B,ref}[k] \tag{11}$$

Then, the thrust magnitude is bounded between a minimum and maximum values, such as:

$$0 < T_{min} \leq ||\mathbf{T}_{B,ref}[k]||_2 \leq T_{max} \tag{12}$$

where $T_{min} = 0$ kN and $T_{max} = 600$ kN are the lower and upper bounds, respectively.

However, the optimization problem subjected to the described dynamics and state and control constraints is not convex and must therefore be convexified. In order to do so, the first step is to convert the free-final-time nonlinear continuous-time optimal control problem into an equivalent fixed-final-time nonlinear continuous-time problem. It is achieved in normalizing the time of flight from $t \in [0, t_f]$ to $\tau \in [0, 1]$, where τ is the normalized time of flight. Summarising the nonlinear dynamics as $\dot{\mathbf{x}}(t) = f(\mathbf{x}(t), \mathbf{u}(t))$ with $\mathbf{x}(t) = \begin{bmatrix} m(t) & \mathbf{r}_I^T(t) & \mathbf{v}_I^T(t) & \mathbf{q}_B^I(t)^T & \boldsymbol{\omega}_B^T(t) \end{bmatrix}^T$ the state vector and $\mathbf{u}(t) = \mathbf{T}_{B,ref}(t)$ the control vector, they can be re-written as follows:

$$\dot{\mathbf{x}}(t) = \frac{\mathrm{d}\tau}{\mathrm{d}t}\frac{\mathrm{d}}{\mathrm{d}\tau}\mathbf{x}(t) \tag{13}$$

Therefore, having $\sigma = (\mathrm{d}\tau/\mathrm{d}t)^{-1}$, the normalized nonlinear dynamics are expressed by:

$$\frac{\mathrm{d}}{\mathrm{d}\tau}\mathbf{x}(\tau) = \sigma \cdot f(\mathbf{x}(\tau), \mathbf{u}(\tau)) \tag{14}$$

Moreover, a *spherical* aerodynamic model is used to describe the aerodynamics of the vehicle. This model, introduced by Szmuk *et al.* in Ref.,[12] approximates the relationship between the aerodynamic force and the velocity vector and has the advantage to be easily implementable in the successive convex optimization guidance method. The aerodynamic force $\mathbf{F}_{aero,I}(t)$ is considered always anti-parallel with respect to the velocity $\mathbf{v}_I(t)$ as if the vehicle was subjected to a pure drag force. Assuming that the rocket is axisymmetric, the aerodynamic forces and moments in the vehicle's body-fixed reference frame are expressed by:

$$\begin{aligned} \mathbf{F}_{aero,B}(t) &= -\frac{1}{2}\rho(t)||\mathbf{v}_{air,I}(t)||_2 S_{ref} C_{aero} \mathbf{R}_B^I(t)\mathbf{v}_{air,I}(t) \\ \mathbf{M}_{aero,B}(t) &= [\mathbf{x}_{CP} - \mathbf{x}_{CG}(t)] \times \mathbf{F}_{aero,B}(t) \end{aligned} \tag{15}$$

where C_{aero} is the aerodynamic coefficient matrix defined by $C_{aero} = \text{diag}\left(\begin{bmatrix} c_{a,x} & c_{a,x} & c_{a,x} \end{bmatrix}\right)$ where $c_{a,x} = 0.82$ is a positive scalar assumed constant during all the flight.

Then, the nonlinear re-entry dynamics equations, defined in Eq. (1), are discretized and linearized about the solution of the previous iteration, through a first-order Taylor approximation and the nonconvex constraints are convexified. It involves two state constraints, the norm of the quaternion (Eq. (9)) and the STC (Eq. (10)); and one control contraint, the lower bound of the thrust magnitude (Eq. (12)). The convexification of the Eq. (9) is obtained through a first-order Taylor expansion approximation evaluated about the previous SOCP $(i-1)^{\text{th}}$ iteration:

$$||\mathbf{q}_B^{I,i-1}[k]||_2 + \frac{\mathbf{q}_B^{I,i-1}[k]^T}{||\mathbf{q}_B^{I,i-1}[k]||_2}(\mathbf{q}_B^{I,i}[k] - \mathbf{q}_B^{I,i-1}[k]) = 1 \tag{16}$$

The same method is used for the STC (Eq. (10)). However, due to the $\min(\cdot)$ function, the constraint is approximated as follows:

$$\begin{cases} h_\alpha(\boldsymbol{\xi}^{i-1}[k]) + \left.\dfrac{\partial h_\alpha}{\partial \boldsymbol{\xi}}\right|_{\boldsymbol{\xi}^{i-1}[k]} (\boldsymbol{\xi}^i[k] - \boldsymbol{\xi}^{i-1}[k]) \leq 0, & \text{if } g_\alpha(\boldsymbol{\xi}^{i-1}[k]) < 0 \\ 0, & \text{otherwise} \end{cases} \tag{17}$$

where $\boldsymbol{\xi}^i[k] = \begin{bmatrix} \mathbf{v}_I^i[k]^T & \mathbf{q}_B^{I,i}[k]^T \end{bmatrix}^T$, $k = \{1, ..., K\}$ is the reference trajectory parameters obtained from the SOCP i^{th} iteration. Lastly, it is applied to the lower bound of the thrust magnitude, obtaining the following expression for $k \in [1, K-1]$:

$$\begin{aligned} &h_T(\mathbf{u}[k]) = T_{min} - ||\mathbf{T}_{B,ref}[k]||_2 \\ &h_T(\mathbf{u}^{i-1}[k]) + \left.\frac{\partial h_T}{\partial \mathbf{u}}\right|_{\mathbf{u}^{i-1}[k]} (\mathbf{u}^i[k] - \mathbf{u}^{i-1}[k]) \leq 0 \end{aligned} \tag{18}$$

Finally, the successive convex optimization strategy involves the use of trust regions and virtual controls to prevent unboundedness and artificial infeasibility, respectively. Trust regions implementation allows to limit the deviation between two consecutive iterations. They are defined for state and control vectors but also for the time of flight:

$$\begin{aligned} ||\mathbf{x}^i[k] - \mathbf{x}^{i-1}[k]||_2 + ||\mathbf{u}^i[k] - \mathbf{u}^{i-1}[k]||_2 \leq \Delta^i_{\mathbf{x},\mathbf{u}}[k] \\ ||\sigma^i - \sigma^{i-1}||_2 \leq \Delta^i_\sigma \end{aligned} \tag{19}$$

Virtual controls are additional control inputs $\boldsymbol{\nu}^i$ which allows reaching each point of the solution domain, through dynamics relaxation. All that terms must be penalized in the cost function. For the norm $\Delta^i_{\mathbf{x},\mathbf{u}}$ and for the virtual control vector $\boldsymbol{\nu}^i$, it is needed to define an auxiliary variable, respectively S^i_Δ and $S^i_{\boldsymbol{\nu}}$, to avoid a quadratic term in the cost function joined with an inequality constraint.[20] Therefore, the following constraints are added:

$$\begin{aligned} ||\Delta^i_{\mathbf{x},\mathbf{u}}||_2 \leq S^i_{\Delta_{\mathbf{x},\mathbf{u}}} \\ ||\boldsymbol{\nu}^i||_2 \leq S^i_{\boldsymbol{\nu}} \end{aligned} \tag{20}$$

The objective of the optimal control problem defined is to find the optimal trajectory, subjected to the defined re-entry dynamics and state and control constraints, minimizing the vehicle's fuel

consumption, which corresponds to maximizing the vehicle's final mass. Due to the monotonic behavior of the propellant consumption with respect to time, the time of flight is first selected as the value to be minimized. Therefore, the cost function can be written as follows at each SOCP i^{th} iteration:

$$J_t = \sigma^i + w_{\boldsymbol{\nu}} S^i_{\boldsymbol{\nu}} + w_{\Delta} S^i_{\Delta} + w_{\Delta_\sigma} \Delta^i_{\sigma} \tag{21}$$

where $w_{\boldsymbol{\nu}} = 10^3$, $w_{\Delta} = 1$ and $w_{\Delta_\sigma} = 0.75$ are penalization weights. This algorithm is hereafter referred to as *SCVxTime* 1.

COST FUNCTION AND ALGORITHM DEVELOPMENTS ANALYSIS

This section aims at analyzing the guidance algorithm performance through several developments. First, the selection of the cost function is studied by comparing different implementation: the minimization of the final time as displayed in Eq. (21), the maximization of the final mass, the minimization of the thrust usage and an hybrid configuration. This latter is combining maximization of the final mass and minimization of the thrust usage. Then, since in the algorithm *SCVxTime* 1, the convexification of the nonconvex constraints is achieved through the successive process via first-order Taylor expansion, this section also analyzes the convexification of the constraints through the so-called lossless convexification. Finally, the outputs of the algorithm are also analyzed regarding the selection of the penalization weights for the trust regions and the virtual controls. To summarize, the following implementations are studied:

- Minimum-final-time strategy VS. maximum-final-mass strategy VS. minimum-thrust-usage VS. hybrid configuration.
- First-order Taylor expansion VS. lossless convexification.
- Selection of the penalization weights for trust regions and virtual controls.

Cost Function Selection

As mentioned in the previous section and more precisely in Eq. (21), the minimization of the time of flight was selected as the cost function for the baseline algorithm referred to as *SCVxTime* 1. This choice was made due to the monotonic behavior of the propellant consumption with respect to time, meaning that minimizing the time of flight is equivalent to minimizing the propellant cost function. However, it is still relevant to analyze the performance of other choices of cost function. As a first example, the minimization of the propellant consumption can also be linked to the maximization of the final mass m_f and therefore the cost function can be written as followed:

$$J_{m_f} = -m^i_f + J^i_w \tag{22}$$

where $J^i_w = w_{\boldsymbol{\nu}} S^i_{\boldsymbol{\nu}} + w_{\Delta} S^i_{\Delta} + w_{\Delta_\sigma} \Delta^i_{\sigma}$ is the part of the cost function related to the penalization of the trust regions and virtual controls. Note that through the discretization process, Eq. (22) is then becoming:

$$J_{m_f} = -m[K]^i + J^i_w \tag{23}$$

Moreover, the minimization of the propellant consumption can also directly be linked to the thrust usage throughout the descent flight. This cost function is given by:

$$J_T = \int_0^t ||\mathbf{T}^i_{B,ref}(t)||_2 \, dt + J^i_w \tag{24}$$

This latter is then discretized using the trapezoidal law and expressed by:

$$J_T = J_w^i + \frac{\sigma^{i-1}}{2(K-1)} \sum_{k=1}^{K-2} \left(||\mathbf{T}_{B,ref}^i[k+1]||_2 + ||\mathbf{T}_{B,ref}^i[k]||_2 \right) \tag{25}$$

Finally, another cost function is studied hereafter referred to as *hybrid* which is defined as a combination of the maximization of the final mass and the minimization of the thrust usage. The cost function is given as follows:

$$J_{hybrid} = -w_m m_f^i + w_T \int_0^t ||\mathbf{T}_{B,ref}^i(t)||_2 \, dt + J_w^i \tag{26}$$

where $w_m = 1$ and $w_T = 1$ are penalization weights which can be use to set more emphasis on a specific cost function.

Lossless Convexification

The successive convex optimization process enables to approximate the remaining nonlinearities in the optimal problem defined but can also be used to convexify the nonconvex constraints such as for example the lower bound of the thrust magnitude. In the algorithm *SCVxTime* 1, the first-order Taylor expansion approximation evaluated about the previous SOCP $(i-1)^{\text{th}}$ iteration is also used for the convexification of the nonconvex constraint following (Reference 12). However, lossless convexification can still be used within the successive process.[11,19] It consists in defining a slack variable $\Gamma(t)$ with the following constraint:

$$||\mathbf{T}_{B,ref}(t)||_2 \leq \Gamma(t) \tag{27}$$

and therefore Eq. (11) becomes:

$$\cos(\delta_{max}) \, \Gamma^i[k] \leq \mathbf{e}_1 \cdot \mathbf{T}_{B,ref}[k] \tag{28}$$

whereas the nonconvex constraint described in Eq. (12) is convexified as follows:

$$T_{min} \leq \Gamma^i[k] \leq T_{max} \tag{29}$$

Note that Eq. (28) (and therefore also Eq. (11)) can be replaced or enhanced with a thrust slew rate constraint defined by:

$$-\dot{T}_{max} \leq \frac{(\Gamma^i[k+1] - \Gamma^i[k]) \cdot (K-1)}{\sigma^{i-1}} \leq \dot{T}_{max} \tag{30}$$

However, this modification did not show any performance increase in the simulations achieved and is therefore not considered in this analysis. Finally, through lossless convexification, J_T of Eq. (24) and Eq. (25) and J_{hybrid} of Eq. (26), are also modified considering the new slack variable Γ. Therefore, the modifications from Eq. (18) to Eq. (20) are applied to *SCVxTime* 1 hereafter called *LosslessTime* 1.

Penalization Weights Selection and Summary

In *SCVxTime* 1 and *LosslessTime* 1 algorithms, three penalization weights are considered; $w_{\boldsymbol{\nu}} = 10^3$, $w_{\Delta} = 1$ and $w_{\Delta_\sigma} = 0.75$, in order to penalize respectively the virtual controls usage, as well as the trust regions regarding the state and control vectors and the time of flight. This weights selection has a relatively high impact in the obtained reference trajectory. In order to assess their impact on the performance, another set of penalization weights is considered: $w_{\boldsymbol{\nu}} = 10^5$, $w_{\Delta} = 0.1$ and $w_{\Delta_\sigma} = 0.075$. The algorithms using this set become *SCVxTime* 2 and *LosslessTime* 2.

Table 1 summarize all the different cases studied.

Algorithm Developments analysis and Discussion

All the algorithm design configurations are assessed and the performance in terms of final mass and time of flight, as well as the obtained reference profile are compared.

First, the different cost functions and the convexification method used (1$^{\text{st}}$-order Taylor expansion approximation or lossless convexification) are compared for the first set of penalization weights. The results are depicted in Figure 3 where the blue bar gives the time of flight generated by the algorithm while the orange bar gives the final mass of the vehicle. Note that the dry mass of the vehicle is equal to $m_{dry} = 2,750$ kg. From this figure, it can be noticed that the performance related to the convexification method used is similar. In fact, the use of lossless convexification instead of the 1$^{\text{st}}$-order Taylor expansion approximation does not always leads to an increase of the performance and when it is the case, the gain is relatively low. As an example, from what concerns the performance of the minimization of the final time, i.e. *SCVxTime* 1 and *LosslessTime* 1, the second algorithm generates a higher final mass ($6,928 \geq 6,881$ kg) for a similar time of flight. Then, the minimization of the time of flight is also perceived as the best cost function compared to the other cases studied. We actually clearly see the monotonic behavior of the propellant consumption with respect to time since all the other cases ended up with a higher time of flight and therefore

Table 1: Summary of the Algorithm Design Cases Studied

Case Name	SCVx	Lossless	Cost function	Weights selection
SCVxTime 1	✓	—	J_t	$w_{\boldsymbol{\nu}} = 10^3$, $w_{\Delta} = 1$ and $w_{\Delta_\sigma} = 0.75$
SCVxMass 1	✓	—	J_{m_f}	$w_{\boldsymbol{\nu}} = 10^3$, $w_{\Delta} = 1$ and $w_{\Delta_\sigma} = 0.75$
SCVxThrust 1	✓	—	J_T	$w_{\boldsymbol{\nu}} = 10^3$, $w_{\Delta} = 1$ and $w_{\Delta_\sigma} = 0.75$
SCVxHybrid 1	✓	—	J_{hybrid}	$w_{\boldsymbol{\nu}} = 10^3$, $w_{\Delta} = 1$ and $w_{\Delta_\sigma} = 0.75$
LosslessTime 1	—	✓	J_t	$w_{\boldsymbol{\nu}} = 10^3$, $w_{\Delta} = 1$ and $w_{\Delta_\sigma} = 0.75$
LosslessMass 1	—	✓	J_{m_f}	$w_{\boldsymbol{\nu}} = 10^3$, $w_{\Delta} = 1$ and $w_{\Delta_\sigma} = 0.75$
LosslessThrust 1	—	✓	J_T	$w_{\boldsymbol{\nu}} = 10^3$, $w_{\Delta} = 1$ and $w_{\Delta_\sigma} = 0.75$
LosslessHybrid 1	—	✓	J_{hybrid}	$w_{\boldsymbol{\nu}} = 10^3$, $w_{\Delta} = 1$ and $w_{\Delta_\sigma} = 0.75$
SCVxTime 2	✓	—	J_t	$w_{\boldsymbol{\nu}} = 10^5$, $w_{\Delta} = 0.1$ and $w_{\Delta_\sigma} = 0.075$
SCVxMass 2	✓	—	J_{m_f}	$w_{\boldsymbol{\nu}} = 10^5$, $w_{\Delta} = 0.1$ and $w_{\Delta_\sigma} = 0.075$
SCVxThrust 2	✓	—	J_T	$w_{\boldsymbol{\nu}} = 10^5$, $w_{\Delta} = 0.1$ and $w_{\Delta_\sigma} = 0.075$
SCVxHybrid 2	✓	—	J_{hybrid}	$w_{\boldsymbol{\nu}} = 10^5$, $w_{\Delta} = 0.1$ and $w_{\Delta_\sigma} = 0.075$
LosslessTime 2	—	✓	J_t	$w_{\boldsymbol{\nu}} = 10^5$, $w_{\Delta} = 0.1$ and $w_{\Delta_\sigma} = 0.075$
LosslessMass 2	—	✓	J_{m_f}	$w_{\boldsymbol{\nu}} = 10^5$, $w_{\Delta} = 0.1$ and $w_{\Delta_\sigma} = 0.075$
LosslessThrust 2	—	✓	J_T	$w_{\boldsymbol{\nu}} = 10^5$, $w_{\Delta} = 0.1$ and $w_{\Delta_\sigma} = 0.075$
LosslessHybrid 2	—	✓	J_{hybrid}	$w_{\boldsymbol{\nu}} = 10^5$, $w_{\Delta} = 0.1$ and $w_{\Delta_\sigma} = 0.075$

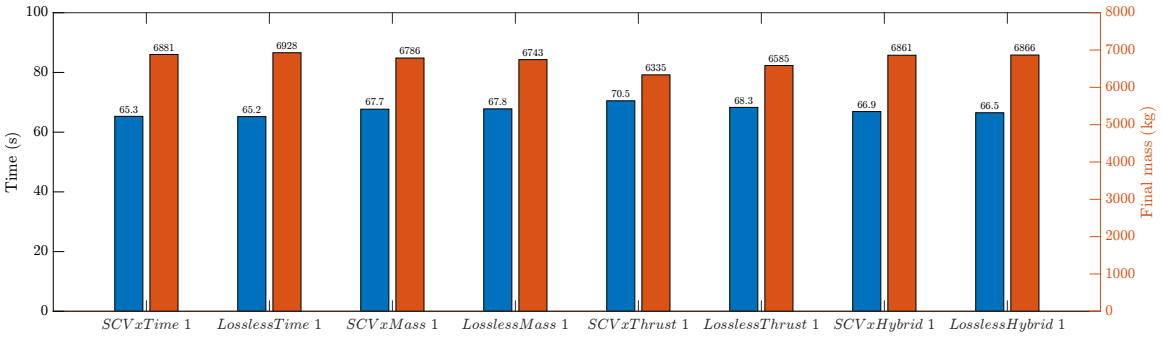

Figure 3: Comparison of the Algorithm Design Cases for the First Set of Penalization Weights

with a lower final mass. Figure 4 shows the obtained thrust profile according to the case studied. More particularly, Figure 4a compared the thrust profile obtained through 1st-order Taylor expansion approximation with the one obtained through lossless convexification for the minimum-time strategy, whereas Figure 4b depicted the thrust profiles obtained through 1st-order Taylor expansion approximation for different cost functions. The thrust profile is relatively similar for all the cases. Figure 4a only shows the minimum-time strategy since the same trend is obtained from the other cost functions and allows to conclude that the convexification method does not have a high impact of the reference thrust profile generation. Figure 4b draws the same conclusion regarding the cost function selection. It is also possible to notice that the profiles are not following the classical bang-bang behavior for rocket powered-descent and landing.[23] Note that the same conclusions can be drawn for the reference pitch angle profile generated but the results are not shown in this paper for a better conciseness.

Then, the same comparison is achieved for the second set of penalization weights. Figure 5 depicts the outputs of this comparison, like Figure 3. From this figure, note that the performance is never as good as the outputs of the first set of penalization weights. In fact, except for the minimum-

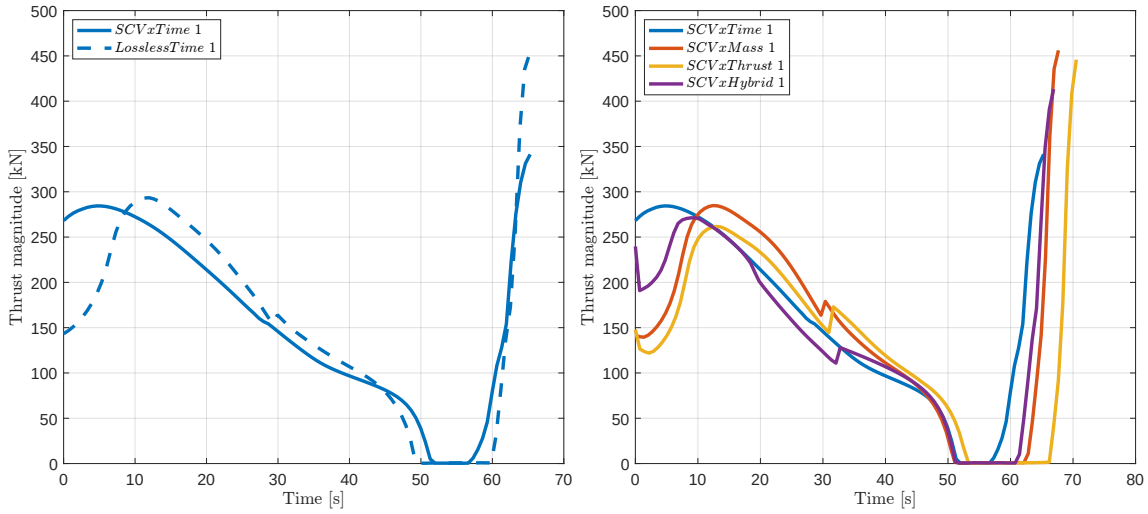

(a) SCVx VS. lossless

(b) Cost function selection

Figure 4: Comparison of the Obtained Thrust Profile for the First Set of Penalization Weights

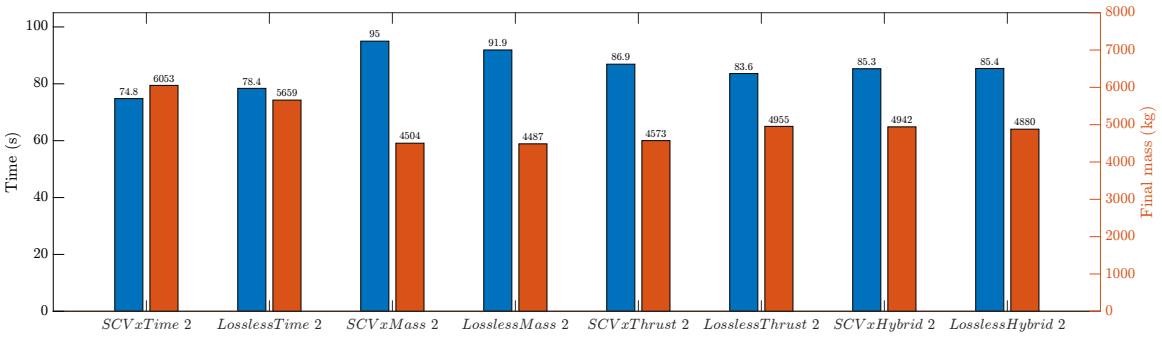

Figure 5: Comparison of the Algorithm Design Cases for the Second Set of Penalization Weights

time strategy, all the other cases shows a significant lower performance than the previous analysis, in terms of time of flight and final mass. However, the same conclusions are drawn: minimum-time strategy still lead to the best performance while the convexification method used is not playing an important role. In the same way, the conclusions regarding the reference thrust and pitch profiles are similar. However, it is interesting to compare the profiles with respect to the ones obtained with the first set of penalization weights. Figure 6 achieves this analysis for the minimum-time strategy. More particularly, Figure 6a shows the reference thrust profiles, whereas Figure 6b the pitch angle profiles. The obtained reference profiles show a significant difference. In fact, the profiles generated by the second set of penalization weights is closer to the classical bang-bang behavior. Even if the time of flight is higher, the final mass is slight lower than the one indicated by the algorithms with the first set of penalization weights. In case of discrepancies due to disturbances, nonlinearities, and/or uncertainties, this type of profile could lead to better performance when considering a closed-loop RLV re-entry nonlinear simulation. The next section will study this impact. Finally, the reference pitch angle profiles depicted in Figure 6b are also relatively different. The ones generated by the second set of penalization weights is less smooth as it shows several slight pitch angle oscillations.

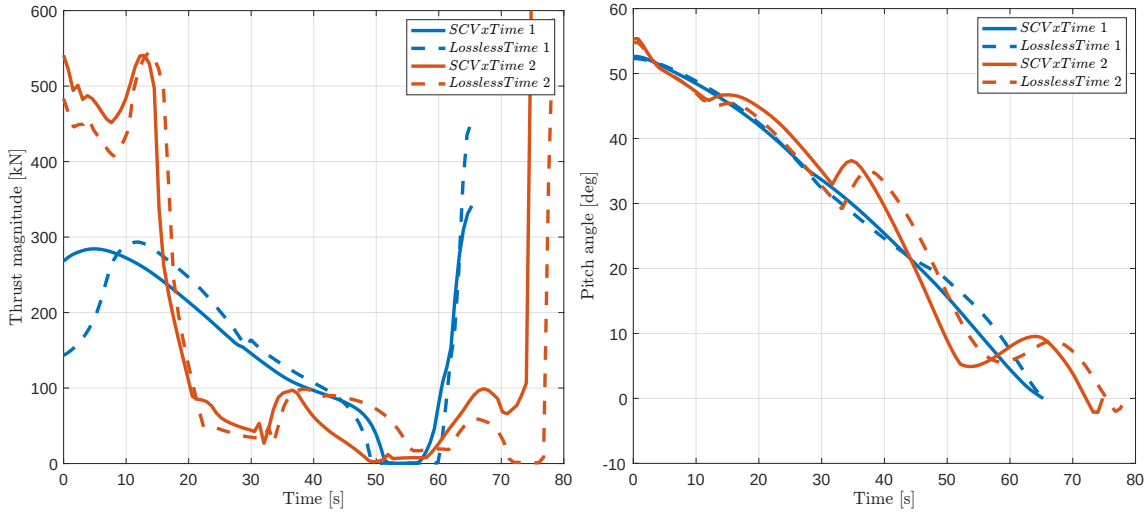

(a) Reference thrust profile

(b) Reference pitch angle profile

Figure 6: Comparison of the Obtained Reference Profiles for the Two Set of Penalization Weights

SIMULATION RESULTS AND DISCUSSION

In this section, the best-performing algorithms are assessed in the 6-DoF reusable launchers re-entry controlled dynamics simulator described previously. More particularly, the four minimum-time strategies are compared: *SCVxTime* 1, *LosslessTime* 1, *SCVxTime* 2, *LosslessTime* 2. Then, several cost function strategies are assessed in order to test if the minimum-time strategy still lead to the best performance. Note that all these simulations are carried out for a simplified aerodynamics model in order not to generate additional errors which could interfere with the outputs of the analysis carried out. More precisely, the aerodynamics model used in the simulator is also considering a pure drag force with a constant drag coefficient equal to $c_{a,x} = 0.82$. Therefore, a last set of simulations is achieved which considers the enhanced aerodynamic model[15] in the simulator in order to study the robustness of the guidance algorithm to uncertainties in the aerodynamics. Table 2 displays the initial and final conditions of the nominal cases studied.

Table 2: Initial and Final Conditions

(a) Initial conditions

Parameter	Value
$\mathbf{r}_I[0]$	$[25,000 \quad 0 \quad -15,000]^T$ m
$\mathbf{v}_I[0]$	$[-850 \quad -0.1 \quad 950]^T$ m/s
$\boldsymbol{\omega}_B[0]$	$[0 \;\; 0 \;\; 0]^T$ rad/s
$m[0]$	14,000 kg

(b) Final conditions

Parameter	Value
$\mathbf{r}_I[K]$	$[0 \;\; 0 \;\; 0]^T$ m
$\mathbf{v}_I[K]$	$[-5 \;\; 0 \;\; 0]^T$ m/s
$\boldsymbol{\omega}_B[K]$	$[0 \;\; 0 \;\; 0]^T$ rad/s
$\mathbf{q}_B^I[K]$	$[0 \;\; 0 \;\; 0 \;\; 1]^T$

Some enhancements in the simulator have been considered. As explained previously, the solution of the more recent guidance is stored as an online look-up table and is updated every 10 seconds. However, in some cases depending on the actual state of the vehicle, the guidance algorithm is generating an unfeasible trajectory or is not converging to a solution. Therefore the re-entry simulation is worsened or stopped whereas it was still possible to follow the previous trajectories generated with acceptable results. To overcome this issue, some feasibility conditions are implemented after a new guidance update is achieved, and when they are not met, the vehicle keeps following the previously updated reference trajectory which was saved. These feasibility conditions involves: (i) the guidance algorithm must have successfully converged to a solution; (ii) the estimated time of flight must be strictly positive, i.e. $ToF^i > 0$; (iii) the estimated final mass must be strictly superior to the vehicle dry mass, i.e. $m_f^i > m_{dry}$.

Comparison of the Best-performing Guidance Algorithms

As mentioned in the previous section, the best-performing guidance algorithm designs are the ones considering the minimum-time strategy. Therefore, they are here assessed in the nonlinear simulator for a realistic scenario. The performance is analyzed in terms of final mass m_f, final downrange error ϵ_{lat} and final velocity v_f. Figure 7 shows the results of the four simulations achieved, each one in closed-loop with a different guidance algorithm designs: *SCVxTime* 1 in Figure 7a, *LosslessTime* 1 in Figure 7b, *SCVxTime* 2 in Figure 7c, *LosslessTime* 2 in Figure 7d. From these figures, it is possible to notice that the first set of penalization weights is not the algorithm design leading to the biggest final mass, as it was foreseen by the previous tests. In fact,

in both cases, the re-updating of the guidance trajectory leads to a higher time of flight and therefore a bigger propellant consumption in order to reach the desired final states. In what concerns the convexification methods, both enable a similar trajectory and performance. As foreseen from the previous study, the thrust profile followed by the vehicle are quite different according to the set of penalization weights chosen. The classical bang-bang behavior is well seen for the second set and enable a lower propellant consumption, however, it produces a relatively high final velocity which cannot ensure a soft landing. The first set of penalization weights consumes more propellant throughout the flight allowing an acceptable final velocity. Note that the precision related to the final downrange error is relatively big for this set. It is more likely due to a difficult maneuver to be achieved by the actuation system at low altitude. Therefore, either the guidance algorithm should be better designed to prevent the generation of such kind of trajectory, either the tuning of the controllers gains should be improved. As a conclusion, the second set of penalization weights enables

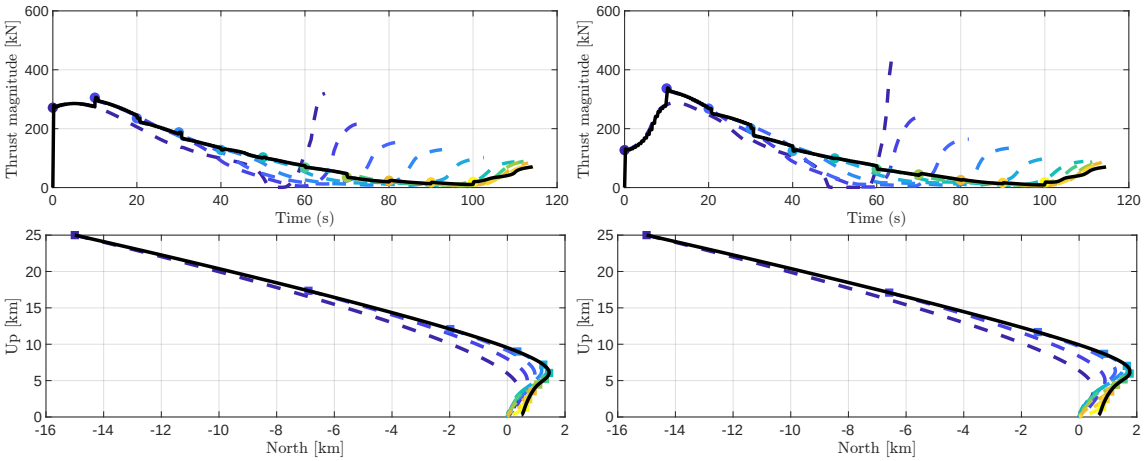

$m_f = 2,803$ kg $e_{lat} = 492$ m $v_f = 9.2$ m/s

(a) *SCVxTime* 1

$m_f = 2,792$ kg $e_{lat} = 682$ m $v_f = 9.0$ m/s

(b) *LosslessTime* 1

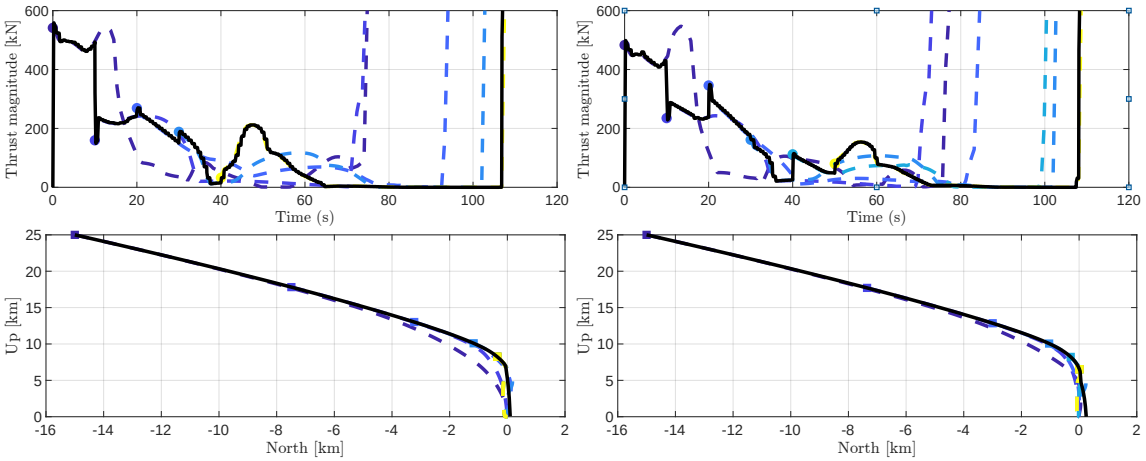

$m_f = 3,794$ kg $e_{lat} = 98$ m $v_f = 20$ m/s

(c) *SCVxTime* 2

$m_f = 3,521$ kg $e_{lat} = 247$ m $v_f = 33$ m/s

(d) *LosslessTime* 2

Figure 7: Comparison of Minimum-Time Strategies through Closed-Loop Nonlinear Simulations

a bang-bang behavior for the thrust profile leading to a lower propellant consumption, as well as a reference trajectory which is easier to be followed by the vehicle in realistic flight conditions. However, the obtained final velocity remains too high. A solution could be to design a proper guidance algorithm for the end of the flight until pinpoint landing (starting for example at an altitude lower than 2 km), as in (Reference 5) where a powered-descent guidance algorithm is used considering only the TVC system as actuator.

Comparison of the Cost Function Strategies

In this subsection, the cost function strategies will be compared for the second set of penalization weights and for the 1st-order Taylor expansion convexification method in order to confirm the highest efficiency of the minimum-time strategy. Therefore, the following algorithm designs are analyzed in closed-loop with the simulator and compared with *SCVxTime* 2: *SCVxMass* 2, *SCVxThrust* 2, and *SCVxHybrid* 2. Figure 8 shows the results of the four simulations achieved. Note that the same observations were made by studying the other set of penalization weights and/or lossless convexification method. From these figures, it is again possible to conclude that the highest performance of the minimum-time strategy foreseen by the previous analysis is not completely confirmed by the nonlinear closed-loop simulations. In fact, in these simulations, the other cost function strategies even lead to a higher final mass. However, the precision and the softness of the landing is not as well ensured since the final downrange position and final velocity errors are higher compared to the minimum-time strategy. Therefore, the minimum-time strategy can be seen as a good compromise between all the critical parameters targeted. Moreover, regarding the minimum-thrust-usage strategy, the reference trajectory to be followed was not recomputed during the flight meaning that the guidance algorithm was not able to converge to a better solution, therefore leading to a re-entry with open-loop guidance. That is why the discrepancies with respect to the targeted values are quite high at the end of the flight. In the other cases, the thrust profiles need a shorter time of flight therefore

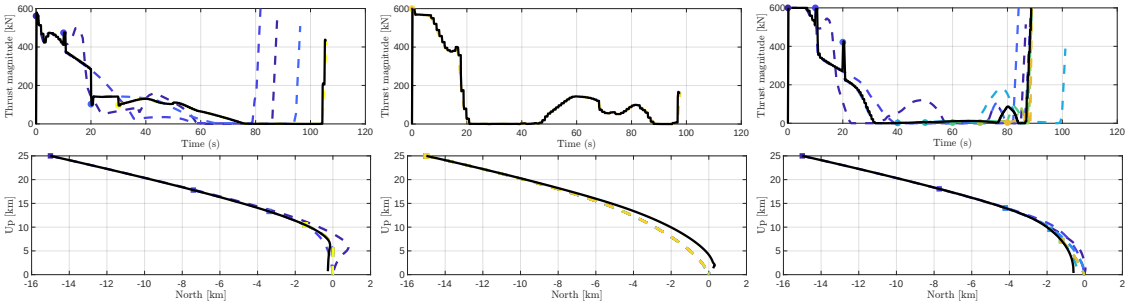

(a) *SCVxMass* 2 (b) *SCVxThrust* 2 (c) *SCVxHybrid* 2

	SCVxMass 2	*SCVxThrust* 2	*SCVxHybrid* 2
Final mass ($\geq 2,750$ kg)	$3,985$ kg	$4,073$ kg	$5,465$ kg
Final downrange position ($= 0$ m)	268 m	235 m	596 m
Final velocity ($= 5$ m/s)	16 m/s	49 m/s	16 m/s

(d) Performance results for the different cost function strategies

Figure 8: Comparison of Cost Function Strategies through Nonlinear Closed-Loop Simulations

reducing the propellant consumption, but on the other hand preventing the vehicle to correct the existing mismatches. Note that the latter can also come from a non-adequate tuning of the controllers gains. Finally, from this analysis, it was concluded that the minimum-time strategy was more flexible in real-time implementation since the time of flight is directly linked with all the others critical parameters.

Aerodynamics Consideration

At the start of this section, it was mentioned that a simplified aerodynamic model accounting for a pure drag force was used in order not to generate errors in the analysis. In this subsection, the enhanced aerodynamic model developed in (Reference 15) is implemented in the nonlinear simulator. This latter updates the aerodynamic coefficients and therefore the aerodynamic force and moment generated by the vehicle according to the vehicle aerodynamic angles and the Mach number. Therefore any modification of the trajectory of the vehicle has an incidence of the aerodynamics. In order to cope with this non-negligible effect, the successive convex optimization can be used to predict the aerodynamic force and moment that the vehicle will encountered.

Recalling Eq. (15) where the aerodynamic force and moment considered in the guidance algorithm is computed from a user-specified aerodynamic coefficient matrix C_{aero}. Let's consider the diagonal coefficient $c_{a,x}$ as a varying parameter which can be computed as follows:

$$c^i_{a,x}[k] = C^i_D[\alpha = \pi, M^i[k]] \tag{31}$$

where $C^i_D(\alpha(t), M(t))$ is the drag coefficient which is estimated from the available lookup tables. Therefore, this enhancement is embedded in the guidance logic described previously and the obtained guidance algorithm is tested through nonlinear closed-loop simulations. All the difference guidance strategies were assessed and the one giving the best results was *LosslessTime* 2. The results are shown in Figure 9. The trajectory profile as well as the altitude VS. velocity profile are depicted respectively at the top and bottom left. From them, it can be noticed that the vehicle is moving smoothly towards the landing site following the computed reference trajectory. The vehicle

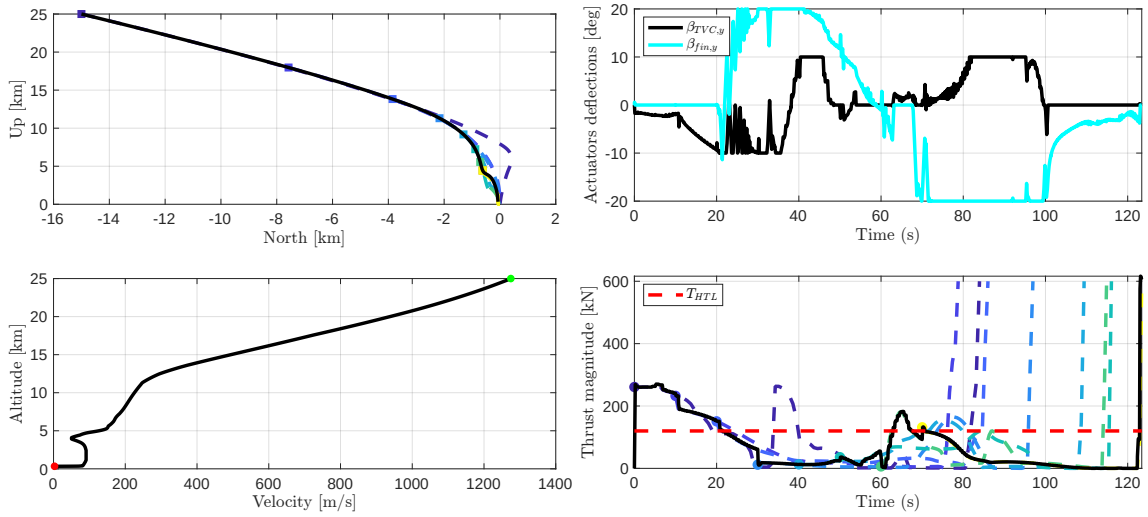

$$m_f = 4,063 \text{ kg} \quad e_{lat} = 67 \text{ m} \quad v_f = 2.8 \text{ m/s}$$

Figure 9: Performance Results of the Closed-Loop Simulations Considering Aerodynamics

is properly slowed down at the end of the flight, reaching a final velocity low enough to ensure a soft landing. On the right, the control inputs are depicted with the TVC gimbal angles and the planar fins deflection angles at the top, as well as the reference thrust magnitude profile at the bottom. The red dashed-line displays the thrust magnitude limit; when the required thrust magnitude is higher than this threshold, the TVC system is primarily used with respect to the steerable planar fins, and conversely. The thrust magnitude profile follows a bang-bang behavior optimizing the propellant consumption. It is relevant to notice that the global performance of this simulation is better than all the other simulations tested, whereas the vehicle final mass is higher. Therefore, the guidance algorithm well managed to use the aerodynamics as an additional control authority to steer the vehicle towards the landing site. The slight discrepancy in the downrange error is more likely due to the saturation of the actuators. As a conclusion of this analysis, successive convex optimization is proven as a good candidate to counteract the aerodynamics encountered for rocket atmospheric re-entry, powered-descent and landing.

CONCLUSIONS

This paper aims at studying advanced guidance algorithm designs for the 6-DoF atmospheric re-entry of reusable launchers. More particularly, successive convex optimization was embedded into the guidance logic and different algorithm designs are analyzed. This guidance method enables to iteratively solve convex optimization SOCP subproblems in which the nonconvex dynamics and constraints are repeatedly linearized using the information coming the previous iteration solution. As an example, this technique allows the consideration of the aerodynamics. Therefore inside this guidance logic, several algorithm developments are analyzed in order to find the optimal design leading to the best performance. Moreover, they are also assessed through a nonlinear 6-DoF reusable launchers re-entry controlled dynamics simulator embedding the guidance logic in a closed-loop fashion with a control system and the RLV flight mechanics involved.

First of all, the cost function strategy is analyzed through four cases: minimum-time formulation, maximum-final-mass, minimum-thrust-usage and an hybrid formulation considering both maximum-final-mass and minimum-thrust-usage. From this study, the minimum-time strategy was selected as the best-performing formulation but also as the most flexible one towards a soft pinpoint landing. In fact, the minimization of the time of flight is linked to the minimization of the propellant consumption due to its monotonic behavior with respect to time.

Then, the convexification method to convexify the lower bound of the thrust magnitude is analyzed through the 1^{st}-order Taylor expansion and the lossless convexification techniques. From this analysis, it was observed that both methods were leading to similar results.

Moreover, the user-specified set of penalization weights also plays an important role in the performance of the guidance algorithm. Two sets are compared, one leading to a shorter time of flight and a bigger final mass, and the other leading to the classical bang-bang behavior of the thrust magnitude profile. The latter enables a lower propellant consumption in closed-loop simulations but usually leads to a high final velocity. A solution to this problem could be to separate the atmospheric re-entry and landing into several phases with particularly a last one at low altitude where a powered-descent guidance algorithm is used with only TVC as actuator.

Finally, the aerodynamics consideration is embedded into the guidance logic and the simulation carried out shows that the guidance strategy well enable to counteract the aerodynamics and to steer the vehicle towards the landing site. Moreover, it is relevant to notice that the case considering the

aerodynamics leads to a better global performance compared to the other algorithm designs, more likely due to the fact that the aerodynamics can also be used to slow down the vehicle and therefore increasing the available control authority to correct the trajectory of the vehicle.

Note that the remaining discrepancies are probably due to the need for an adequate tuning of the controllers gains, here using gain-scheduled PID controllers. Future work will study the implementation of structured H_∞ control method towards an enhanced robustness to uncertainties.

ACKNOWLEDGMENT

The project leading to this application has received funding from the European Union's Horizon 2020 research and innovation programme under the Marie Skłodowska-Curie grant agreement No 860956.

REFERENCES

[1] L. Blackmore, "Autonomous Precision Landing of Space Rockets," *The Bridge on Frontiers of Engineering*, Vol. 4, No. 46, 2016, pp. 15–20.

[2] M. Wall, "Wow! SpaceX Lands Orbital Rocket Successfully in Historic First," 2015.

[3] Rocket Lab, "Rocket Lab Electron 'Its a Test' flight successfully makes it to space," 2017.

[4] P. Simplício, A. Marcos, and S. Bennani, "Reusable Launchers: Development of a Coupled Flight Mechanics, Guidance, and Control Benchmark," *Journal of Spacecraft and Rockets*, Vol. 57, jan 2020, pp. 74–89, 10.2514/1.a34429.

[5] M. Sagliano, A. Heidecker, J. M. Hernández, S. Farì, M. Schlotterer, S. Woicke, D. Seelbinder, and E. Dumont, "Onboard Guidance for Reusable Rockets: Aerodynamic Descent and Powered Landing," *AIAA Scitech 2021 Forum*, American Institute of Aeronautics and Astronautics, jan 2021, 10.2514/6.2021-0862.

[6] A. R. Klumpp, "Apollo lunar descent guidance," *Automatica*, Vol. 10, mar 1974, pp. 133–146, 10.1016/0005-1098(74)90019-3.

[7] J. C. Harpold and D. E. Gavert, "Space Shuttle entry guidance performance results," *Journal of Guidance, Control, and Dynamics*, Vol. 6, nov 1983, pp. 442–447, 10.2514/3.8523.

[8] B. Açıkmeşe and S. R. Ploen, "Convex Programming Approach to Powered Descent Guidance for Mars Landing," *Journal of Guidance, Control, and Dynamics*, Vol. 30, sep 2007, pp. 1353–1366, 10.2514/1.27553.

[9] B. Açıkmeşe, M. Aung, J. Casoliva, S. Mohan, A. E. Johnson, D. P. Scharf, D. A. Masten, J. Scotkin, A. Wolf, and M. W. Regehr, "Flight testing of trajectories computed by G-FOLD: Fuel optimal large divert guidance algorithm for planetary landing," *23rd AAS/AIAA Space Flight Mechanics Meeting, Kauai, HI*, 2013.

[10] D. Malyuta, Y. Yu, P. Elango, and B. Açıkmeşe, "Advances in trajectory optimization for space vehicle control," *Annual Reviews in Control*, Vol. 52, 2021, pp. 282–315, 10.1016/j.arcontrol.2021.04.013.

[11] X. Liu, "Fuel-Optimal Rocket Landing with Aerodynamic Controls," *Journal of Guidance, Control, and Dynamics*, Vol. 42, jan 2019, pp. 65–77, 10.2514/1.g003537.

[12] M. Szmuk, T. P. Reynolds, and B. Açıkmeşe, "Successive Convexification for Real-Time Six-Degree-of-Freedom Powered Descent Guidance with State-Triggered Constraints," *Journal of Guidance, Control, and Dynamics*, Vol. 43, aug 2020, pp. 1399–1413, 10.2514/1.g004549.

[13] M. Sagliano, "Generalized hp Pseudospectral-Convex Programming for Powered Descent and Landing," *Journal of Guidance, Control, and Dynamics*, Vol. 42, jul 2019, pp. 1562–1570, 10.2514/1.g003731.

[14] A. De Oliveira and M. Lavagna, "Reusable Launchers Re-entry Controlled Dynamics Simulator," Proceedings of the 9th European Conference for Aeronautics and Aerospace Sciences. Lille, France, 27th June - 1st July 2022, 2022, 10.13009/EUCASS2022-6193.

[15] A. De Oliveira and M. Lavagna, "Assessment of Reusable Launch Vehicles Re-entry Dynamics Control Effectiveness with Enhanced Aerodynamics Modelling," Proceedings of the 73rd International Astronautical Congress (IAC), Paris, France, 18th - 22nd September 2022, 2022.

[16] E. Mooij, *The motion of a vehicle in a planetary atmosphere*. Faculty of Aerospace Engineering, Delft University of Technology, 1994.

[17] Committee on Extension to the Standard Atmosphere, "U.S. Standard Atmosphere 1976," Technical Memorandum NASA-TM-X-74335, NASA, October 1976.

[18] M. Szmuk, B. Acikmese, and A. W. Berning, "Successive Convexification for Fuel-Optimal Powered Landing with Aerodynamic Drag and Non-Convex Constraints," *AIAA Guidance, Navigation, and Control Conference*, American Institute of Aeronautics and Astronautics, jan 2016, 10.2514/6.2016-0378.

[19] P. Simplício, A. Marcos, and S. Bennani, "Guidance of Reusable Launchers: Improving Descent and Landing Performance," *Journal of Guidance, Control, and Dynamics*, Vol. 42, oct 2019, pp. 2206–2219, 10.2514/1.g004155.

[20] J. Guadagnini, M. Lavagna, and P. Rosa, "Model predictive control for reusable space launcher guidance improvement," *Acta Astronautica*, oct 2021, 10.1016/j.actaastro.2021.10.014.

[21] M. Grant and S. Boyd, "CVX: MATLAB Software for Disciplined Convex Programming, version 2.1," `http://cvxr.com/cvx`, Mar. 2014.

[22] A. Domahidi, E. Chu, and S. Boyd, "ECOS: An SOCP solver for embedded systems," *2013 European Control Conference (ECC)*, IEEE, jul 2013, 10.23919/ecc.2013.6669541.

[23] T. P. Reynolds and M. Mesbahi, "Optimal Planar Powered Descent with Independent Thrust and Torque," *Journal of Guidance, Control, and Dynamics*, Vol. 43, jul 2020, pp. 1225–1231, 10.2514/1.g004701.